THE UNIVERSITY OF
WARWICK

Original citation:
LHCb Collaboration (Including: Back, J. J., Dossett, D., Gershon, T. J., Harrison, P. F., Kreps, Michal, Latham, Thomas, Pilar, T., Poluektov, Anton, Reid, M. M., Silva Coutinho, R., Whitehead, M. and Williams, M. P.). (2012) Measurement of charged particle multiplicities in pp collisions at root s=7 TeV in the forward region. European Physical Journal C, Volume 72 (Number 4). Article number 1947.

Permanent WRAP url:
http://wrap.warwick.ac.uk/54615

warwick**publications**wrap

highlight your research

http://wrap.warwick.ac.uk/

Regular Article - Experimental Physics

Measurement of charged particle multiplicities in *pp* collisions at $\sqrt{s} = 7$ TeV in the forward region

The LHCb Collaboration[⋆]

CERN, 1211 Geneva 23, Switzerland

Abstract Charged particle production in proton-proton collisions is studied with the LHCb detector at a centre-of-mass energy of $\sqrt{s} = 7$ TeV in different intervals of pseudorapidity η. Charged particles are reconstructed close to the interaction region in the vertex detector, which provides high reconstruction efficiency in the η ranges $-2.5 < \eta < -2.0$ and $2.0 < \eta < 4.5$. The data were taken with a minimum bias trigger, only requiring one or more reconstructed tracks in the vertex detector. By selecting an event sample with at least one track with a transverse momentum greater than 1 GeV/c a hard QCD subsample is investigated. Several event generators are compared with the data; none are able to describe fully the multiplicity distributions or the charged particle density distribution as a function of η. In general, the models underestimate charged particle production.

1 Introduction

Charged particle multiplicity is a basic observable that characterizes the hadronic final state. The multiplicity distribution is sensitive to the underlying QCD dynamics of the proton-proton collision. ALICE [1], ATLAS [2] and CMS [3] have measured charged multiplicity distributions mainly covering the central region, while LHCb's geometrical acceptance allows the dynamics of the collision to be probed in the forward region. The forward region is in particular sensitive to low Bjorken-x QCD dynamics and multiparton interactions (MPI) [4].

In this analysis, charged particles are reconstructed in the vertex detector (VELO) surrounding the interaction region. The VELO was designed to provide a uniform acceptance in the forward region with additional coverage of the backward region. In the absence of almost any magnetic field in the VELO region, the particle trajectories are straight lines and

therefore no acceptance corrections as a function of momentum are needed. Since the VELO is close to the interaction region, the amount of material before the particle detection is small, minimising the corrections for particle interactions with detector material.

This paper is organized as follows. Section 2 gives a brief description of the LHCb detector and the configuration used to record data in Spring 2010. The Monte Carlo simulation and data selection are outlined in Sects. 3 and 4 respectively, with Sect. 5 giving an overview of the analysis. The systematic uncertainties are outlined in Sect. 6. The final results are discussed in Sect. 7 and compared with different model expectations, before concluding in Sect. 8.

2 LHCb detector

The LHCb detector is a single-arm magnetic dipole spectrometer with a polar angular coverage with respect to the beam line of approximately 15 to 300 mrad in the horizontal bending plane, and 15 to 250 mrad in the vertical non-bending plane. The detector is described in detail elsewhere [5]. A right-handed coordinate system is defined with its origin at the nominal proton-proton interaction point, the z axis along the beam line and pointing towards the magnet, and the y axis pointing upwards.

For the low luminosity running period of the LHC relevant for this analysis, the probability of observing more than one collision in a proton-proton bunch crossing (*pile-up*) is measured to be (3.7 ± 0.4) %, dominated by a double interaction. For the measurements presented in this paper the tracking detectors are of particular importance. The LHCb tracking system consists of the VELO surrounding the proton-proton interaction region, a tracking station (TT) before the dipole magnet, and three tracking stations (T1–T3) after the magnet. Particles traversing from the interaction region to the downstream tracking stations experience an integrated bending-field of approximately 4 Tm.

⋆e-mail: n.brook@bristol.ac.uk

The VELO consists of silicon microstrip modules, providing a measure of the radial and azimuthal coordinates, r and ϕ, distributed in 23 stations arranged along the beam direction. The first two stations at the most upstream z positions are instrumented to provide information on the number of visible interactions in the detector at the first level of the trigger. The VELO is constructed in two halves, movable in the x and y directions so that it can be centered on the beam. During stable beam conditions the two halves are located at their nominal closed position, with active silicon only 8 mm from the beams, providing full azimuthal coverage.

The TT station also uses silicon microstrip technology. The T1–T3 tracking stations have silicon microstrips in the region close to the beam pipe, whereas straw tubes are employed in the outer region.

Though the particle multiplicity is measured using only tracks reconstructed with the VELO, momentum information is only available for "long" tracks. Long tracks are formed from hits in the VELO (before the magnet) and in the T1–T3 stations (after the magnet). If available, measurements in the TT station are added to the long track.

The LHCb trigger system consists of two levels. The first level is implemented in hardware and is designed to reduce the event rate to a maximum of 1 MHz. The complete detector is then read out and the data is sent to the second level, a software trigger. For the early data taking period with low luminosity used in this analysis a simplified trigger was used. The first level trigger made no decision and the events were passed through to the higher level trigger. A fast track reconstruction was performed in the software trigger and events with at least one track observed in the VELO were accepted.

3 Monte Carlo simulation

Monte Carlo event simulation is used to correct for acceptance, resolution effects and for background characterisation. The detector simulation is based on the GEANT4 [6] package. Details of the detector simulation are given in Ref. [5]. The distribution of material in the simulation of the VELO's component parts was compared with that measured at the time of production and agreement was found to be within 15 %. The largest component of the material budget of the VELO is the thin foil that separate the beam and detector vacuum. This has a very complex shape and has to be approximated in its description. The Monte Carlo event samples are passed through reconstruction and selection procedures identical to those for the data.

Elastic and inelastic proton-proton collisions are generated using the PYTHIA 6.4 event generator [7], with CTEQ6L parton density functions [8], which is tuned to

lower energy hadron collider data [9]. The inelastic processes include both single and double diffractive components. The decay of the generated particles is carried out by EvtGen [10], with final state radiation handled by PHOTOS [11]. Secondary particles produced in material interactions are decayed through the GEANT4 program.

4 Data selection

A sample of 3×10^6 events, collected during May 2010, was used in this analysis. In order to minimize the contribution of secondary particles and misreconstructed (fake) tracks, only the tracks satisfying a set of minimal quality criteria are accepted. To minimise fake tracks a cut on the χ^2 per degree of freedom of the reconstructed track, $\chi^2/\text{ndf} < 5$, is applied. To further reduce fake tracks, and reduce duplicate tracks due to splitting of the reconstructed trajectory, a cut of less than four missing VELO hits compared to the expectation is applied. To ensure that tracks originate from the primary interaction, the requirements $d_0 < 2$ mm and $z_0 < 3\sigma_L$ are applied, where d_0 is the track's closest distance to the beam line, z_0 is the distance along the z direction from the centre of the luminous region and σ_L is the width of the luminous region, averaged over the data period, extracted from a Gaussian fit. The run-to-run variation in σ_L is insignificant for the analysis.

Tracks are considered for this analysis only if their pseudorapidity is in either of the ranges $-2.5 < \eta < -2.0$ or $2.0 < \eta < 4.5$. Pseudorapidity is defined as $-\ln[\tan(\theta/2)]$ where θ is the polar angle of the particle with respect to the z direction. The forward range is divided in five equal subintervals with $\Delta\eta = 0.5$.

5 Analysis strategy

The reconstructed multiplicity distributions are corrected on an event by event basis to account for the tracking and selection efficiencies and for the background contributions. These corrected distributions are then used to measure the charged particle multiplicities in each of the η intervals (bins) through an unfolding procedure. Only events with tracks in the η bins are included in the distributions and subsequent normalisation. The distributions are corrected for pile-up effects so they represent charged particle multiplicities, n_{ch}, for single proton–proton interactions. No unfolding procedure is required for the charged particle pseudorapidity density distribution i.e. the mean number of charged particles per single pp-collision and unit of pseudorapidity. Only corrections for background and track efficiency are applied. For this distribution, at least one VELO track is required in
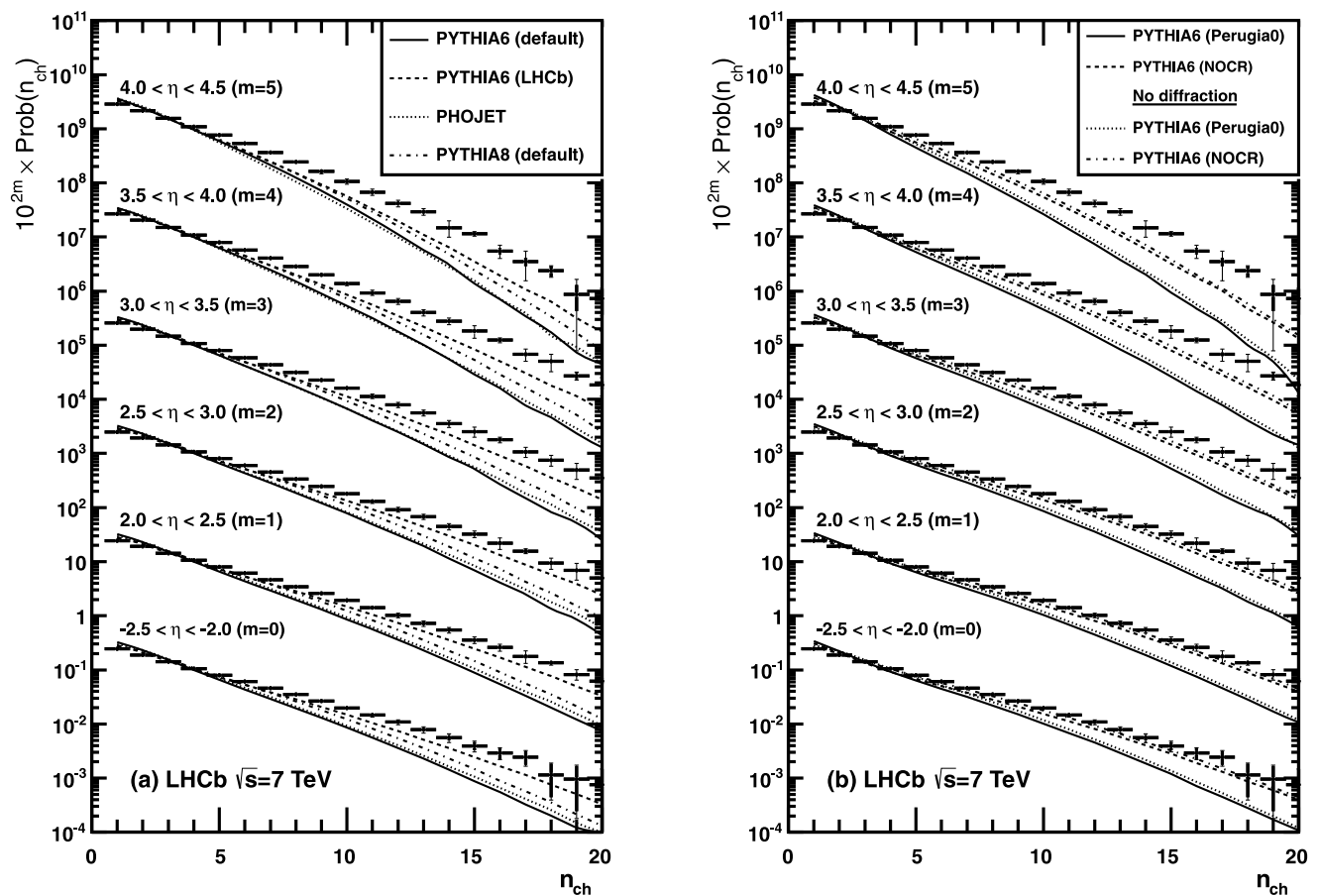
Fig. 1 The multiplicity distribution in η bins (shown as *points* with statistical *error bars*) with predictions of different event generators. The *inner error bar* represents the statistical uncertainty and the *outer error bar* represents the systematic and statistical uncertainty on the

measurements. The data in both figures are identical with predictions from PYTHIA 6, PHOJET and PYTHIA 8 in (**a**) and predictions of the PYTHIA 6 Perugia tunes with and without diffraction in (**b**)

the full forward η range. Each of element of the analysis procedure is discussed in subsequent subsections.

Hard interaction events are defined by requiring at least one long track with $p_T > 1$ GeV/c in the range $2.5 < \eta < 4.5$ where the detector has high efficiency. The geometric acceptance is no longer independent of momentum and therefore the distributions require an additional correction.

In this analysis primary charged particles are defined as all particles for which the sum of the ancestors' mean lifetimes is shorter than 10 ps; according to this definition the decay products of beauty and charm are primary particles.

5.1 Efficiency correction

The LHCb simulation is used to estimate the overall tracking and selection efficiency as a function of pseudorapidity and azimuthal angle ϕ. It is found that the efficiency (including acceptance) in the forward region is typically greater than 90 % while it is at least 85 % in the backward region. Tracking efficiency depends weakly on the event track mul-

tiplicity; this is taken into account in the evaluation of the systematic error.

5.2 Background contributions

There are two main sources of background that can affect the measurement of the multiplicity of charged particles: secondary particles misidentified as primary and fake tracks. Other sources of background, such as beam-gas interactions, are estimated to be negligible.

The correlation between the number of VELO hit clusters in an event and its track multiplicity is in good agreement between the data and simulation, indicating that the fraction of fake tracks is well understood. It is also found that for each η bin the multiplicity of fake tracks is linearly dependent on the number of VELO clusters in the event. Therefore it is possible to parameterise the fake contribution as a function of VELO clusters using the Monte Carlo simulation.

The majority of secondary particles are produced in photon conversions in the VELO material, and in the decay of
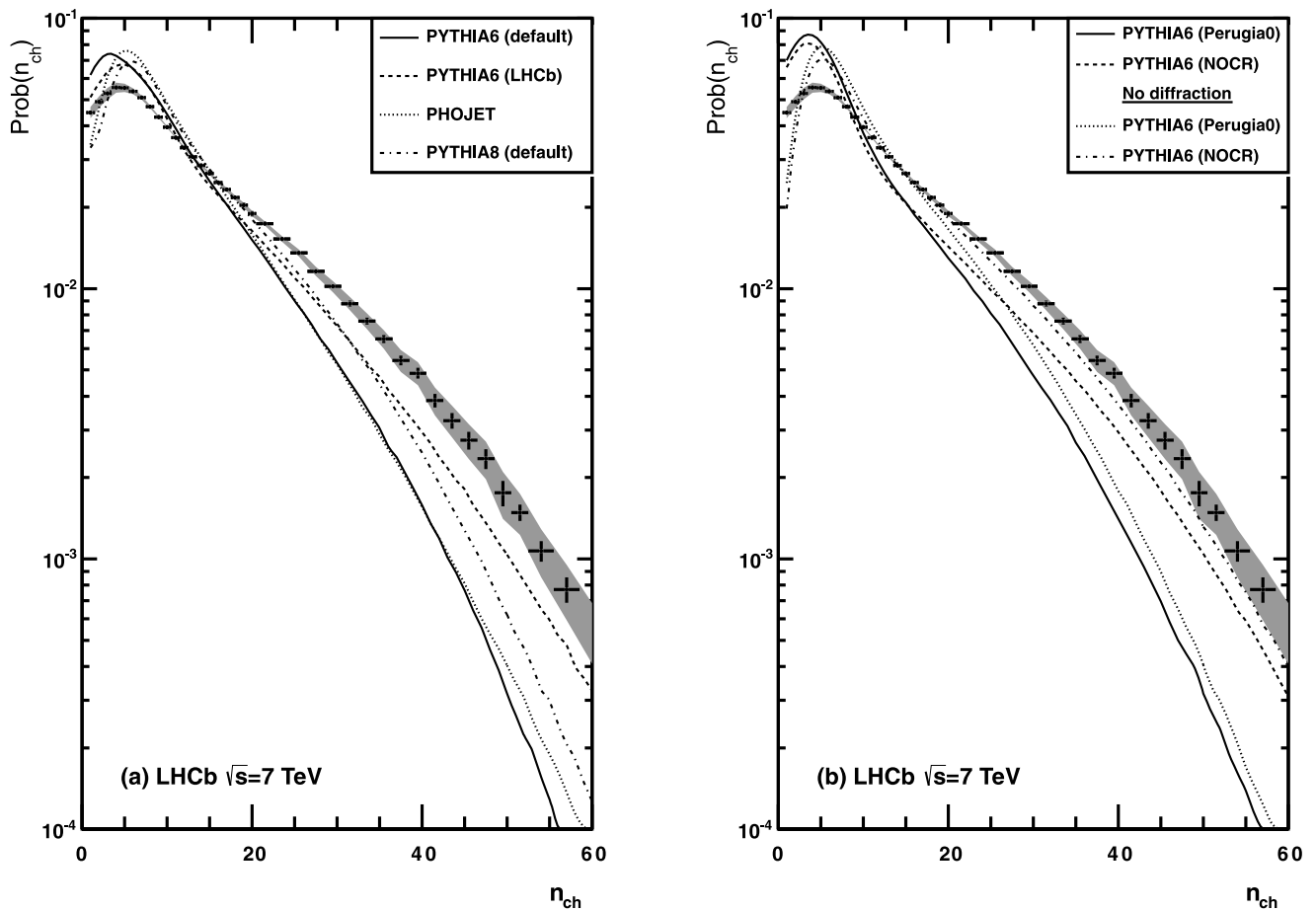
Fig. 2 The multiplicity distribution in the forward η range (shown as *points* with *error bars*) with predictions of different event generators. The *shaded bands* represent the total uncertainty on the measurements.

The data in both figures are identical with predictions from PYTHIA 6, PHOJET and PYTHIA 8 in (**a**) and predictions of the PYTHIA 6 Perugia tunes with and without diffraction in (**b**)

long-lived strange particles such as K_S^0 and hyperons. While earlier LHCb measurements show that the production of K_S^0 is reasonably described by the Monte Carlo generator [12], there are indications that the production of Λ particles is underestimated [13]. This difference is accounted for in the systematic error associated with the definition of primary particles.

The fraction of secondary particles is estimated as a function of both η and ϕ. In general, depending on the η bin, the correction for non-primary particles (from conversion and secondaries) changes the mean values of the particle multiplicity distributions by 5–10 %.

5.3 Correction and unfolding procedure

The procedure consists of three steps; a background subtraction is made, followed by an efficiency correction and finally a correction for pile-up. The procedure is applied to all measured track multiplicity distributions in each of the different η intervals.

In the first step, the distribution is corrected for fake tracks and non-primary particles. A mean number of background tracks is estimated for each event based on the parameterizations described in Sect. 5.2. A PDF (probability density function) is built with this mean value assuming a Poisson distribution for the number of background tracks, m_{bkgnd}. From this PDF the probability to have m_{bkgnd} tracks can be calculated. Using this information a PDF for the number of prompt charged particles, given the number of measured tracks, can be calculated on an event by event basis. These per event PDFs are summed up and normalized to obtain the reconstructed prompt charged track multiplicity distribution i.e. the fraction of events with n_{tr} tracks, Prob(n_{tr}).

In the second step, the correction for the tracking efficiency is applied. For each η bin a mean efficiency, ϵ, is calculated based on the per track efficiency as function of (η, ϕ). As explained below, this is used to unfold the background-subtracted track multiplicity distribution, Prob(n_{tr}), to obtain the underlying charged particle multiplicity distribution, Prob($\tilde{n}_{ch}$), where $\tilde{n}_{ch}$ is the number of
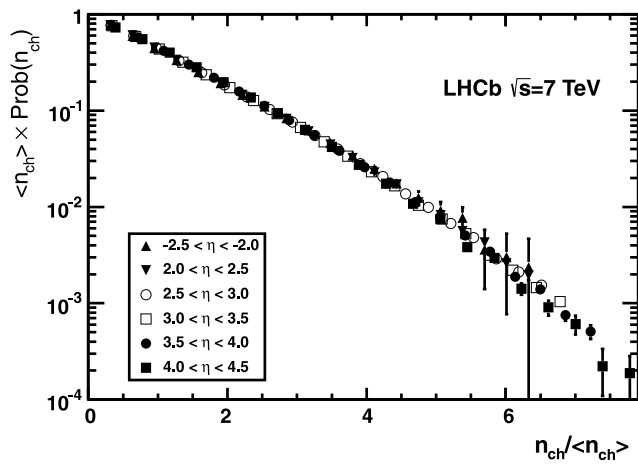
Fig. 3 The KNO distributions in different bins of η. Only the statistical uncertainties are shown

primary produced particles of all proton-proton collisions in an event.

For a given value of $\tilde{n}_{ch}$, the probability to observe n_{tr} reconstructed tracks given a reconstruction efficiency ϵ is described by the binomial distribution

$$p(n_{tr}, \tilde{n}_{ch}, \epsilon) = \binom{\tilde{n}_{ch}}{n_{tr}} (1 - \epsilon)^{\tilde{n}_{ch} - n_{tr}} \epsilon^{n_{tr}}. \tag{1}$$

Hence, the observed track multiplicity distribution is given by

$$\text{Prob}(n_{tr}) = \sum_{\tilde{n}_{ch}=0}^{\infty} \text{Prob}(\tilde{n}_{ch}) \times p(n_{tr}, \tilde{n}_{ch}, \epsilon). \tag{2}$$

The values for $\text{Prob}(\tilde{n}_{ch})$ are obtained by performing a fit to $\text{Prob}(n_{tr})$. The procedure has been verified using simulated data and is in agreement to better than 5 per mille.

In the last step, the distributions are corrected for pile-up to obtain charged particle multiplicity distributions of single interaction events, $\text{Prob}(n_{ch})$. This is done using an iterative procedure. For low luminosity, $\text{Prob}(\tilde{n}_{ch})$ has mainly two contributions: single proton-proton interactions, $P(n_{ch})$, and a convolution of two single proton-proton interactions, $\sum_{k=0}^{n_{ch}} \text{Prob}(k) \times \text{Prob}(k - n_{ch})$. The starting assumption is that the observed distribution is the single proton-proton interaction. From this, the convolution term is calculated, and by subtracting it from the observed distribution, a first order estimate for the single proton-proton distribution is obtained. This can then be used to calculate again the convolution term and obtain a second order estimate for the single proton-proton distribution. The procedure usually converges after the second iteration. The pile-up correction typically changes the mean value of the particle multiplicity distributions by 3–4 %. It was checked that the contribution from pile-up events with more than two proton-proton collisions is negligible.
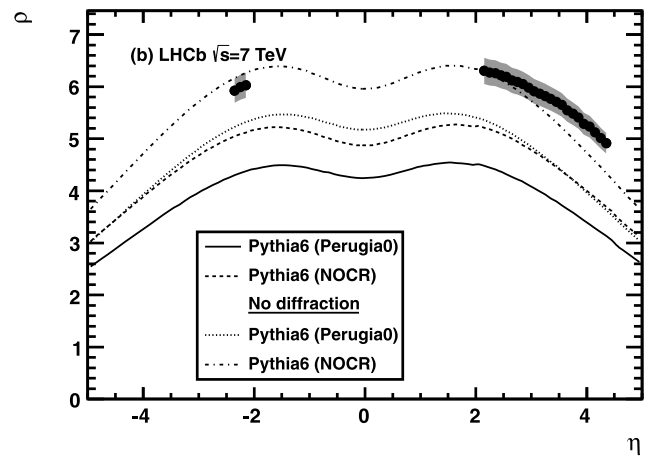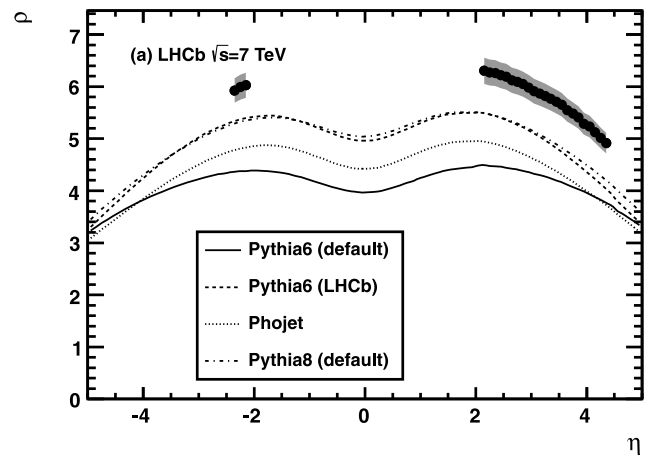

Fig. 4 The charged particle densities as a function of η (shown as *points* with statistical *error bars*) and comparisons with predictions of event generators, as indicated in the key. The *shaded bands* represent the total uncertainty. The events are selected by requiring at least one charged particle in the range $2.0 < \eta < 4.5$. The data in both figures are identical with predictions from PYTHIA 6, PHOJET and PYTHIA 8 in (**a**) and predictions of the PYTHIA 6 Perugia tunes with and without diffraction in (**b**)

As mentioned before, no unfolding procedure is required for the charged particle pseudorapidity density, only the per track corrections for background tracks and tracking efficiency are applied. The distribution is then normalized to the total number of proton-proton collisions including pile-up collisions. In the case of hard interactions, the pseudorapidity density distribution of the pile-up collisions without the p_T cut is first subtracted. Finally, the distribution is normalized to the total number of hard collisions.

6 Systematic uncertainty

6.1 Efficiency

Studies based on data and simulation show that the error on the tracking efficiency for particles reaching the tracking sta-

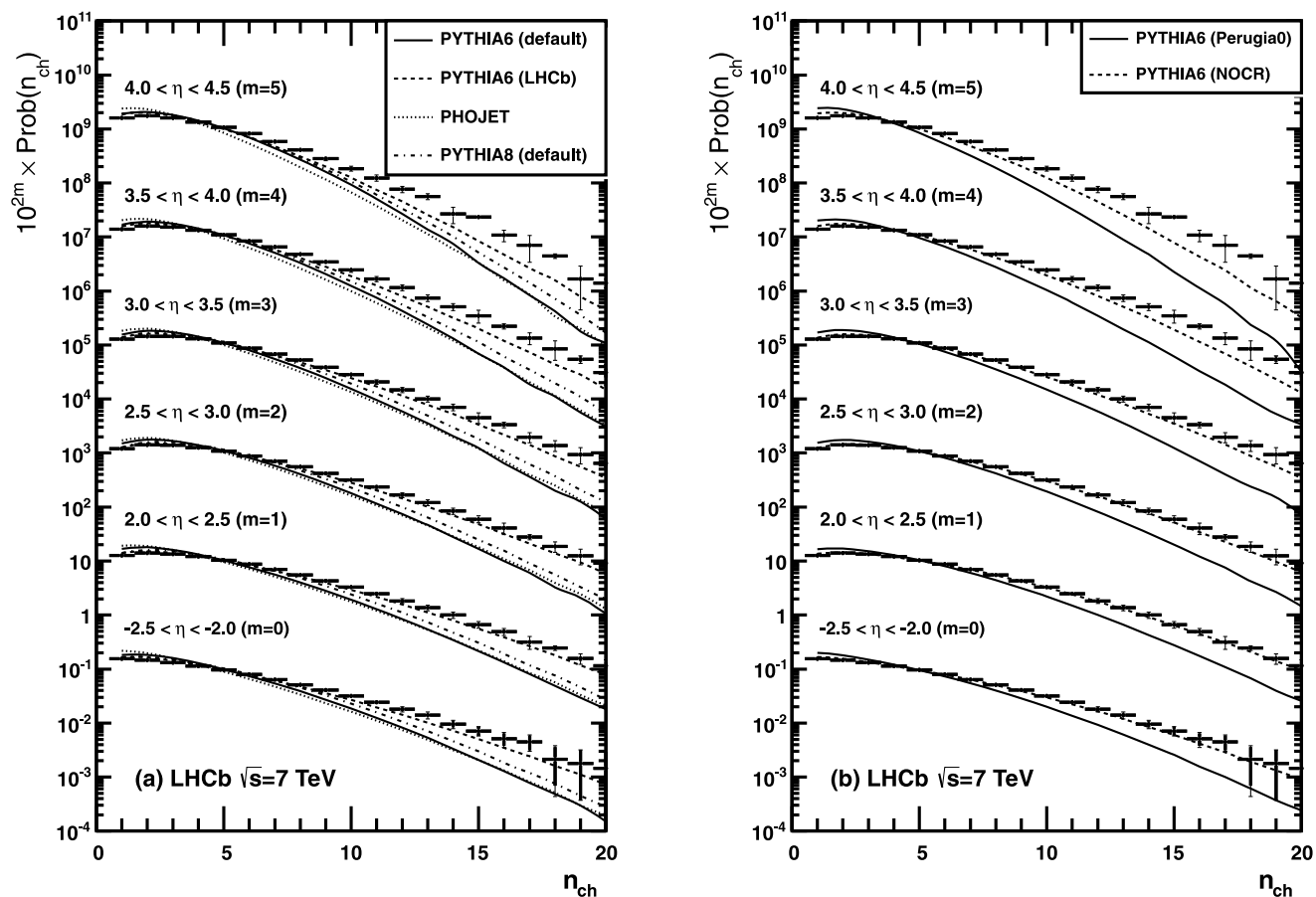**Fig. 5** The multiplicity distribution in η bins (shown as *points* with *error bars*) with predictions of different event generators. The *inner error bar* represents the statistical uncertainty and the *outer error bar* represents the systematic and statistical uncertainty on the measurements.

The events have at least one track with a $p_T > 1.0$ GeV/c in the pseudorapidity range $2.5 < \eta < 4.5$. The data in both figures are identical with predictions from PYTHIA 6, PHOJET and PYTHIA 8 in (**a**) and predictions of the PYTHIA 6 Perugia tunes in (**b**)

tions T1–T3 is <3 % [14]. The tracking efficiency reduces for low-momentum ($p_T < 50$ MeV/c) particles due to interactions with the detector material and the residual magnetic field in the VELO region. Since no momentum measurement exists for the reconstructed VELO tracks, the estimate of a mean efficiency relies on the prediction of the LHCb Monte Carlo model for the contribution of low-momentum particles to the total number of particles. The simulation predicts that in the forward region the fraction of particles below a transverse momentum of 50 MeV/c is 2.4 %. The corresponding average single track efficiency in this η range is measured to be 94 %. In the two extreme cases in which no particles with p_T below 50 MeV/c were reconstructed or no such particles were produced the average track efficiency would be reduced by 1.2 % or increased by 1.1 % respectively. Assuming a 25 % uncertainty on the number of low momentum particles, as suggested by the comparison between the measured particle multiplicity and Monte Carlo prediction, the additional contribution to the track efficiency uncertainty is <1 %. Adding this to the 3 % track recon-

struction uncertainty, gives an overall 4 % error on the track efficiency used in the unfolding procedure. The systematic error contribution is then estimated by unfolding the multiplicity distributions varying the tracking efficiency by ±4 %.

6.2 Non-primary particles

The main systematic uncertainty on the contribution of non-primary particles arises from the knowledge of the detector material (15 %). Two thirds of non-primary particles are due to conversions of photons from π^0 decays, resulting in an 10 % uncertainty. The multiplicity of π^0 scales with the charged multiplicity and as the corrections applied are parameterised as a function of the measured number of tracks no additional error for fake tracks is applied. Varying by ±40 % the production of Λ results in an uncertainty of about 5 % on the non-primary contribution. A pessimistic assumption of a 25 % underestimation of the non-prompt contribution would change the mean and RMS values of the particle multiplicity distributions by −2 %, which can be neglected compared to the tracking efficiency uncertainty of 4 %.
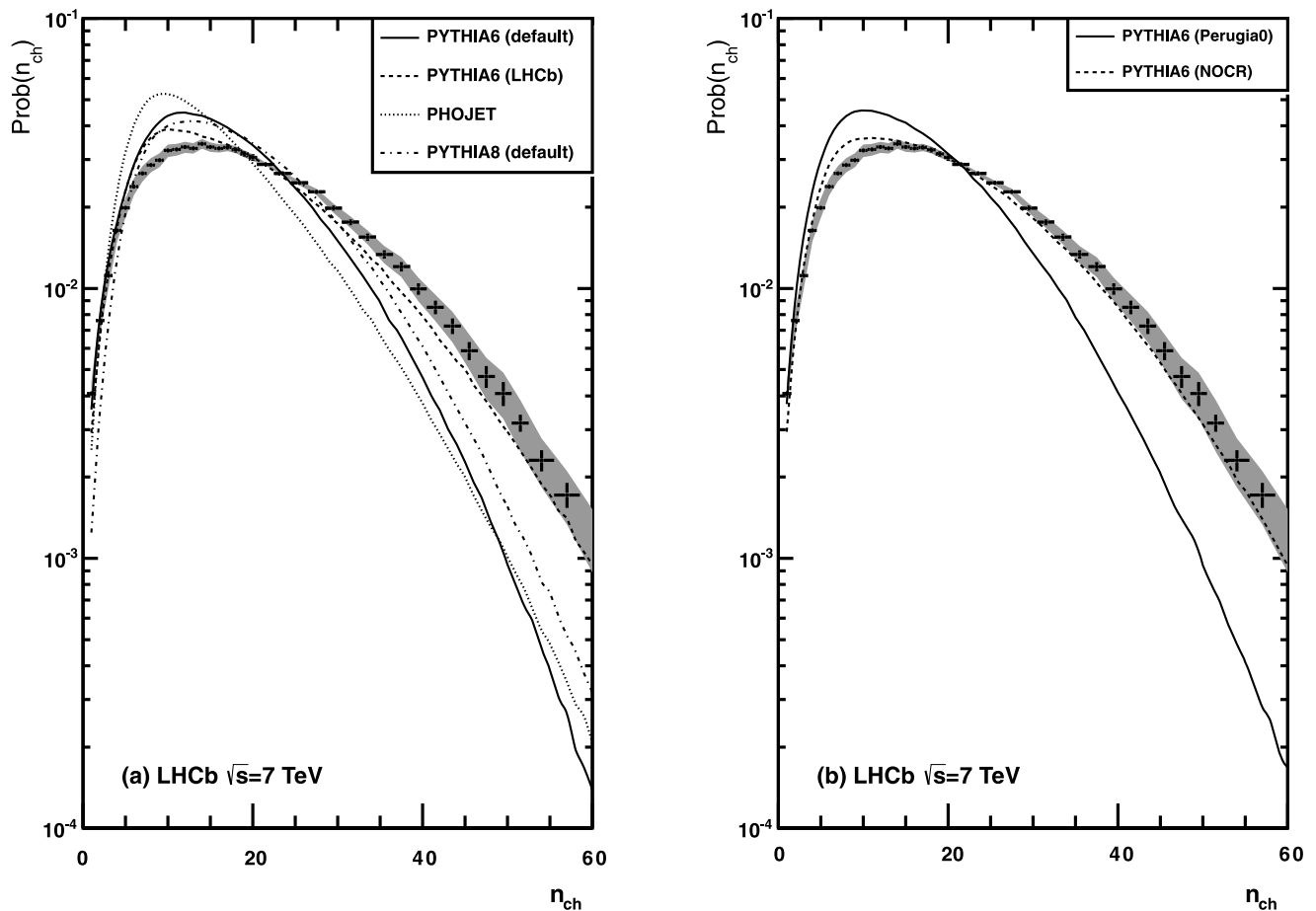
Fig. 6 The multiplicity distribution in the forward η range (shown as *points* with statistical *error bars*) with predictions of different event generators. The *shaded bands* represent the total uncertainty. The events have at least one track with a $p_T > 1.0$ GeV/c in the pseudo-

rapidity range $2.5 < \eta < 4.5$. The data in both figures are identical with predictions from PYTHIA 6, PHOJET and PYTHIA 8 in (**a**) and predictions of the PYTHIA 6 Perugia tunes in (**b**)

6.3 Pile-up

The pile-up corrections inherit a systematic uncertainty from the determination of the mean number of visible interactions of 10 %. This correction to the pile-up fraction is small and is negligible compared to the systematic uncertainty due to the track efficiency correction.

7 Results

Figure 1 shows unfolded charged particle multiplicity distribution for different bins in pseudorapidity, η. Figure 2 shows multiplicity distributions for the full forward range, $2.0 < \eta < 4.5$. There is a requirement of at least one track in the relevant η range. The distributions are compared to several Monte Carlo event generators. PYTHIA 6.424 is compared with the data for a number of tunes including the LHCb tuned settings [9]. In particular the Perugia0 and PerugiaNOCR tunings [15] are shown. In addition, the

PYTHIA 8.145 generator [16] was compared to the data as well as PHOJET 1-12.35 [17]. In general all generators underestimate the multiplicity distributions, with the LHCb tune giving the best description of the data; this tune does not use data from the LHC. The exclusion of the PYTHIA diffractive processes in the Perugia tunes, Figs. 1b and 2b, also improves the description of the data, particularly in the full forward region. Tables of the multiplicity data are given in the Appendix (Tables 1–7).

The Koba–Nielsen–Olesen (KNO) scaling variable [18] has been used to compare the data in the different η bins. Figure 3 shows the KNO scaled multiplicity distributions, $\Psi(u) = \langle n_{ch} \rangle \times \text{Prob}(n_{ch})$ as a function of $u = \frac{n_{ch}}{\langle n_{ch} \rangle}$. As the multiplicity distributions measured are truncated the mean used was extracted by fitting a negative binomial distribution. It clearly shows that the distributions in the different η bins are equivalent. In particular this illustrates that when there is a requirement of at least one track in the η bin the forward and backward regions ($2.0 < |\eta| < 2.5$) are identical.

The charged particle pseudorapidity density, ρ, is shown as a function of pseudorapidity in Fig. 4. The data have a marked asymmetry between the forward and backward region; this is a consequence of the requirement of at least one track in the full forward η range. All models fail to describe the mean charged particle multiplicity per unit of pseudorapidity. The models, to varying degrees, also display the asymmetry but in none of the models is this as large as in the data. The effect on the predictions of excluding diffractive processes is shown in Fig. 4b using the Perugia tunes. There is a better description of the η distribution in the backward directions but it still fails to describe the forward-backward asymmetry.

A sample of hard QCD events were studied by ensuring at least one track in the pseudorapidity range $2.5 < \eta < 4.5$ has a transverse momentum $p_T > 1$ GeV/c. In comparison to the data without this p_T requirement, the multiplicity distributions have larger high multiplicity tails, see Figs. 5 and 6. The data are again compared to predictions of several event generators. In general the predictions are in better agreement than for the minimum bias data but the pseudorapidity range $4.0 < \eta < 4.5$ remains poorly described. As the p_T cut removes the majority of diffractive events from PYTHIA 6 the comparisons with and without diffraction are not shown. Again tables of the multiplicity data are given in the Appendix (Tables 1–7).

The charged particle density as a function of pseudorapidity for the hard QCD sample is shown in Fig. 7. The discontinuity observed in the data at $\eta = 2.5$ is an artefact of the event selection for the hard events. The asymmetry between the forward and backward region is further amplified in this sample. All models fail to describe the mean charged particle multiplicity per unit of pseudorapidity. The models, to varying degrees, also display the asymmetry but never give an effect as large as the data. The Perugia (NOCR) tune gives the best description of the data in the backward direction but fails to reproduce the size of the asymmetry.

8 Summary

The LHCb spectrometer acceptance, $2.0 < \eta < 4.5$, allows the forward region to be probed at the LHC. Charged multiplicity distributions at $\sqrt{s} = 7$ TeV are measured with and without a p_T event selection, making use of the high efficiency of the LHCb VELO. Several event generators are compared to the data; none are fully able to describe the multiplicity distributions or the charged density distribution as a function of η in the LHCb acceptance. In general, the models underestimate charged particle production, in agreement with the measurements in the central region at the LHC.
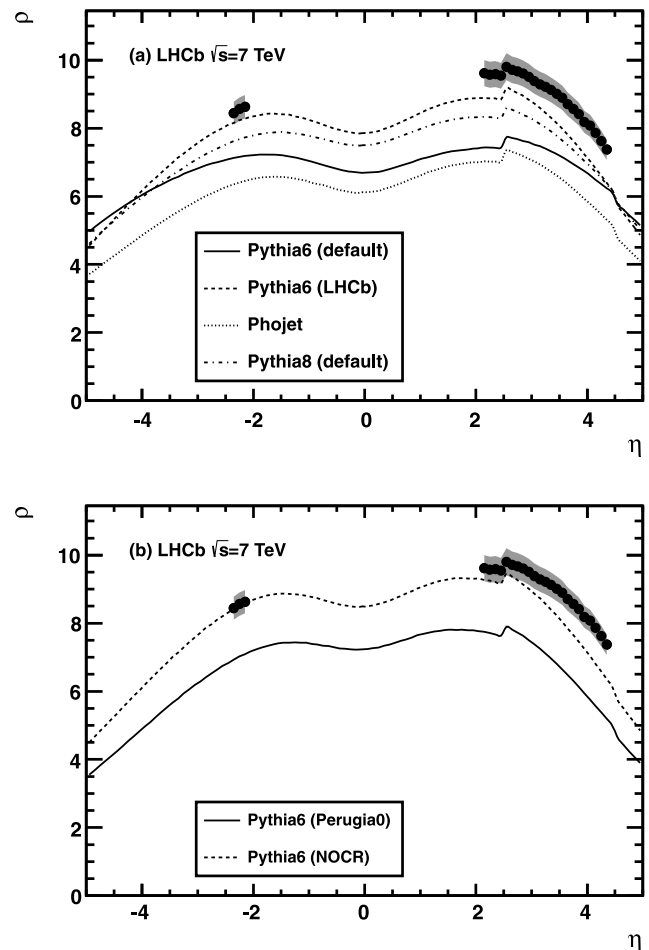

Fig. 7 The data charged particle densities as a function of η (shown as *points* with statistical *error bars*) and comparisons with predictions of event generators, as indicated in the key. The events have at least one track with a $p_T > 1.0$ GeV/c in the pseudorapidity range $2.5 < \eta < 4.5$. The *shaded bands* represent the total uncertainty

Appendix: Tables of charged particle multiplicities

Table 1 Charged particle multiplicity distribution in the pseudorapidity range $-2.5 < \eta < -2.0$ for minimum bias events and for hard QCD events (see text). The first quoted uncertainty is statistical and the second is systematic

n_{ch}	Prob. in min. bias events $\times 10^3$	Prob. in hard QCD events $\times 10^3$
1	$246.66 \pm 0.40 \pm 7.96$	$155.54 \pm 0.49 \pm 6.47$
2	$188.43 \pm 0.41 \pm 4.03$	$146.92 \pm 0.55 \pm 5.26$
3	$141.00 \pm 0.41 \pm 1.25$	$132.46 \pm 0.61 \pm 3.20$
4	$105.57 \pm 0.42 \pm 0.11$	$114.15 \pm 0.67 \pm 1.75$
5	$79.25 \pm 0.43 \pm 0.75$	$96.44 \pm 0.73 \pm 0.24$
6	$60.83 \pm 0.45 \pm 1.13$	$79.84 \pm 0.79 \pm 0.48$
7	$46.08 \pm 0.48 \pm 1.33$	$63.40 \pm 0.83 \pm 1.33$
8	$35.01 \pm 0.50 \pm 1.35$	$51.30 \pm 0.90 \pm 1.63$
9	$26.43 \pm 0.52 \pm 1.40$	$40.66 \pm 0.97 \pm 1.81$
10	$19.75 \pm 0.55 \pm 1.36$	$31.50 \pm 1.02 \pm 1.86$
11	$14.60 \pm 0.57 \pm 1.19$	$24.16 \pm 1.08 \pm 1.83$
12	$10.82 \pm 0.59 \pm 1.00$	$18.03 \pm 1.12 \pm 1.64$
13	$7.86 \pm 0.61 \pm 0.90$	$13.96 \pm 1.21 \pm 1.61$
14	$5.57 \pm 0.63 \pm 0.86$	$9.56 \pm 1.19 \pm 1.28$
15	$3.94 \pm 0.65 \pm 0.73$	$7.14 \pm 1.30 \pm 1.09$
16	$2.90 \pm 0.67 \pm 0.37$	$5.10 \pm 1.29 \pm 1.11$
17	$2.44 \pm 0.68 \pm 0.96$	$4.48 \pm 1.34 \pm 1.28$
18	$1.14 \pm 0.70 \pm 0.61$	$2.13 \pm 1.43 \pm 2.03$
19	$0.96 \pm 0.71 \pm 0.66$	$1.78 \pm 1.41 \pm 0.19$
20	$0.75 \pm 0.72 \pm 0.27$	$1.46 \pm 1.44 \pm 0.60$

Table 2 Charged particle multiplicity distribution in the pseudorapidity range $2.0 < \eta < 2.5$ for minimum bias events and for hard QCD events (see text). The first quoted uncertainty is statistical and the second is systematic

n_{ch}	Prob. in min. bias events $\times 10^3$	Prob. in hard QCD events $\times 10^3$
1	$244.35 \pm 0.36 \pm 7.66$	$126.88 \pm 0.38 \pm 6.57$
2	$191.00 \pm 0.33 \pm 4.02$	$140.50 \pm 0.43 \pm 5.81$
3	$142.72 \pm 0.31 \pm 1.44$	$133.83 \pm 0.44 \pm 3.91$
4	$106.75 \pm 0.28 \pm 0.10$	$121.45 \pm 0.44 \pm 1.95$
5	$80.27 \pm 0.26 \pm 0.73$	$103.10 \pm 0.43 \pm 0.75$
6	$61.09 \pm 0.25 \pm 1.22$	$86.87 \pm 0.42 \pm 0.98$
7	$46.22 \pm 0.23 \pm 1.42$	$70.01 \pm 0.41 \pm 1.59$
8	$34.57 \pm 0.21 \pm 1.45$	$55.15 \pm 0.39 \pm 1.83$
9	$26.09 \pm 0.20 \pm 1.38$	$43.12 \pm 0.36 \pm 2.13$
10	$19.30 \pm 0.18 \pm 1.34$	$32.71 \pm 0.34 \pm 2.20$
11	$14.08 \pm 0.17 \pm 1.17$	$24.64 \pm 0.32 \pm 2.00$
12	$10.17 \pm 0.16 \pm 1.07$	$18.25 \pm 0.29 \pm 1.80$
13	$7.23 \pm 0.14 \pm 0.98$	$13.66 \pm 0.28 \pm 1.84$
14	$5.43 \pm 0.13 \pm 0.82$	$9.97 \pm 0.25 \pm 1.52$
15	$3.55 \pm 0.12 \pm 0.60$	$6.64 \pm 0.22 \pm 1.12$
16	$2.60 \pm 0.11 \pm 0.40$	$4.91 \pm 0.21 \pm 0.78$
17	$1.78 \pm 0.10 \pm 0.65$	$3.14 \pm 0.18 \pm 1.23$
18	$1.35 \pm 0.09 \pm 0.28$	$2.45 \pm 0.17 \pm 0.47$
19	$0.82 \pm 0.08 \pm 0.22$	$1.56 \pm 0.15 \pm 0.42$
20	$0.62 \pm 0.07 \pm 0.19$	$1.15 \pm 0.13 \pm 0.34$

Table 3 Charged particle multiplicity distribution in the pseudorapidity range $2.5 < \eta < 3.0$ for minimum bias events and for hard QCD events (see text). The first quoted uncertainty is statistical and the second is systematic

n_{ch}	Prob. in min. bias events $\times 10^3$	Prob. in hard QCD events $\times 10^3$
1	$249.37 \pm 0.35 \pm 7.88$	$121.02 \pm 0.36 \pm 6.72$
2	$194.45 \pm 0.33 \pm 4.11$	$140.71 \pm 0.41 \pm 6.20$
3	$144.53 \pm 0.29 \pm 1.39$	$138.90 \pm 0.42 \pm 4.26$
4	$107.18 \pm 0.27 \pm 0.10$	$125.71 \pm 0.41 \pm 2.10$
5	$80.42 \pm 0.24 \pm 0.89$	$108.13 \pm 0.40 \pm 0.34$
6	$60.29 \pm 0.22 \pm 1.34$	$87.75 \pm 0.37 \pm 1.24$
7	$45.03 \pm 0.20 \pm 1.53$	$70.69 \pm 0.35 \pm 1.85$
8	$33.53 \pm 0.18 \pm 1.55$	$55.79 \pm 0.33 \pm 2.31$
9	$24.75 \pm 0.16 \pm 1.46$	$42.12 \pm 0.30 \pm 2.40$
10	$17.98 \pm 0.15 \pm 1.30$	$31.82 \pm 0.27 \pm 2.23$
11	$12.98 \pm 0.13 \pm 1.23$	$23.37 \pm 0.25 \pm 2.10$
12	$9.16 \pm 0.12 \pm 1.12$	$16.64 \pm 0.22 \pm 1.95$
13	$6.74 \pm 0.11 \pm 0.87$	$12.07 \pm 0.19 \pm 1.52$
14	$4.46 \pm 0.09 \pm 0.71$	$8.43 \pm 0.17 \pm 1.27$
15	$3.23 \pm 0.08 \pm 0.47$	$5.97 \pm 0.15 \pm 0.88$
16	$2.20 \pm 0.07 \pm 0.71$	$4.07 \pm 0.13 \pm 1.31$
17	$1.57 \pm 0.06 \pm 0.32$	$2.78 \pm 0.11 \pm 0.52$
18	$0.94 \pm 0.05 \pm 0.32$	$1.86 \pm 0.10 \pm 0.51$
19	$0.69 \pm 0.05 \pm 0.33$	$1.26 \pm 0.09 \pm 0.56$
20	$0.50 \pm 0.04 \pm 0.13$	$0.92 \pm 0.08 \pm 0.20$

Table 4 Charged particle multiplicity distribution in the pseudorapidity range $3.0 < \eta < 3.5$ for minimum bias events and for hard QCD events (see text). The first quoted uncertainty is statistical and the second is systematic

n_{ch}	Prob. in min. bias events $\times 10^3$	Prob. in hard QCD events $\times 10^3$
1	$257.54 \pm 0.36 \pm 8.38$	$128.89 \pm 0.38 \pm 7.33$
2	$199.12 \pm 0.33 \pm 4.08$	$145.79 \pm 0.41 \pm 6.39$
3	$147.50 \pm 0.30 \pm 1.23$	$145.41 \pm 0.43 \pm 4.13$
4	$108.21 \pm 0.27 \pm 0.31$	$130.01 \pm 0.42 \pm 2.16$
5	$79.83 \pm 0.24 \pm 1.10$	$109.73 \pm 0.41 \pm 0.44$
6	$58.83 \pm 0.22 \pm 1.50$	$87.48 \pm 0.38 \pm 1.58$
7	$43.25 \pm 0.20 \pm 1.67$	$67.91 \pm 0.35 \pm 2.16$
8	$31.48 \pm 0.18 \pm 1.64$	$52.94 \pm 0.32 \pm 2.50$
9	$22.72 \pm 0.16 \pm 1.48$	$38.50 \pm 0.29 \pm 2.43$
10	$16.12 \pm 0.14 \pm 1.28$	$28.21 \pm 0.26 \pm 2.21$
11	$11.37 \pm 0.13 \pm 1.19$	$20.63 \pm 0.24 \pm 2.17$
12	$7.89 \pm 0.11 \pm 1.07$	$14.74 \pm 0.21 \pm 1.83$
13	$5.63 \pm 0.10 \pm 0.81$	$10.02 \pm 0.18 \pm 1.45$
14	$3.54 \pm 0.08 \pm 0.67$	$7.00 \pm 0.16 \pm 1.02$
15	$2.53 \pm 0.07 \pm 0.71$	$4.49 \pm 0.13 \pm 1.37$
16	$1.79 \pm 0.06 \pm 0.38$	$3.33 \pm 0.12 \pm 0.64$
17	$1.07 \pm 0.06 \pm 0.29$	$1.96 \pm 0.10 \pm 0.53$
18	$0.75 \pm 0.05 \pm 0.17$	$1.38 \pm 0.09 \pm 0.32$
19	$0.49 \pm 0.04 \pm 0.22$	$0.94 \pm 0.08 \pm 0.43$
20	$0.35 \pm 0.04 \pm 0.10$	$0.65 \pm 0.07 \pm 0.17$

Table 5 Charged particle multiplicity distribution in the pseudorapidity range $3.5 < \eta < 4.0$ for minimum bias events and for hard QCD events (see text). The first quoted uncertainty is statistical and the second is systematic

n_{ch}	Prob. in min. bias events $\times 10^3$	Prob. in hard QCD events $\times 10^3$
1	$268.35 \pm 0.37 \pm 8.77$	$139.99 \pm 0.39 \pm 7.61$
2	$206.16 \pm 0.34 \pm 4.00$	$158.42 \pm 0.44 \pm 6.72$
3	$150.62 \pm 0.31 \pm 0.98$	$151.42 \pm 0.45 \pm 4.01$
4	$108.81 \pm 0.28 \pm 0.56$	$133.07 \pm 0.44 \pm 1.67$
5	$78.99 \pm 0.25 \pm 1.35$	$110.17 \pm 0.42 \pm 0.92$
6	$56.92 \pm 0.22 \pm 1.77$	$84.74 \pm 0.38 \pm 1.91$
7	$40.49 \pm 0.20 \pm 1.81$	$65.65 \pm 0.36 \pm 2.61$
8	$28.60 \pm 0.18 \pm 1.68$	$48.06 \pm 0.32 \pm 2.71$
9	$19.98 \pm 0.16 \pm 1.46$	$34.60 \pm 0.29 \pm 2.49$
10	$13.79 \pm 0.14 \pm 1.30$	$24.49 \pm 0.26 \pm 2.26$
11	$9.31 \pm 0.12 \pm 1.18$	$16.62 \pm 0.22 \pm 2.05$
12	$6.48 \pm 0.11 \pm 0.94$	$11.50 \pm 0.19 \pm 1.51$
13	$4.02 \pm 0.09 \pm 0.68$	$7.40 \pm 0.17 \pm 1.18$
14	$2.80 \pm 0.08 \pm 0.41$	$5.09 \pm 0.15 \pm 0.75$
15	$1.82 \pm 0.07 \pm 0.64$	$3.48 \pm 0.13 \pm 1.27$
16	$1.24 \pm 0.06 \pm 0.28$	$2.23 \pm 0.11 \pm 0.45$
17	$0.68 \pm 0.05 \pm 0.25$	$1.35 \pm 0.09 \pm 0.43$
18	$0.50 \pm 0.04 \pm 0.21$	$0.85 \pm 0.08 \pm 0.47$
19	$0.27 \pm 0.04 \pm 0.05$	$0.55 \pm 0.06 \pm 0.14$
20	$0.18 \pm 0.03 \pm 0.08$	$0.31 \pm 0.05 \pm 0.18$

Table 6 Charged particle multiplicity distribution in the pseudorapidity range $4.0 < \eta < 4.5$ for minimum bias events and for hard QCD events (see text). The first quoted uncertainty is statistical and the second is systematic

n_{ch}	Prob. in min. bias events $\times 10^3$	Prob. in hard QCD events $\times 10^3$
1	$284.08 \pm 0.40 \pm 9.11$	$159.68 \pm 0.01 \pm 8.81$
2	$215.09 \pm 0.38 \pm 4.25$	$174.85 \pm 0.01 \pm 6.65$
3	$155.18 \pm 0.35 \pm 0.72$	$159.67 \pm 0.01 \pm 3.42$
4	$109.77 \pm 0.32 \pm 1.07$	$135.15 \pm 0.01 \pm 0.61$
5	$76.74 \pm 0.29 \pm 1.76$	$107.91 \pm 0.01 \pm 1.45$
6	$53.34 \pm 0.27 \pm 1.97$	$82.45 \pm 0.01 \pm 2.49$
7	$36.49 \pm 0.24 \pm 1.93$	$58.82 \pm 0.01 \pm 2.84$
8	$24.57 \pm 0.22 \pm 1.75$	$41.25 \pm 0.01 \pm 2.75$
9	$16.30 \pm 0.20 \pm 1.50$	$28.48 \pm 0.01 \pm 2.55$
10	$10.63 \pm 0.17 \pm 1.25$	$18.52 \pm 0.01 \pm 2.11$
11	$6.76 \pm 0.15 \pm 1.00$	$12.41 \pm 0.01 \pm 1.83$
12	$4.20 \pm 0.13 \pm 0.70$	$7.64 \pm 0.01 \pm 1.25$
13	$2.92 \pm 0.12 \pm 0.57$	$5.63 \pm 0.01 \pm 1.12$
14	$1.48 \pm 0.10 \pm 0.86$	$2.66 \pm 0.01 \pm 1.54$
15	$1.15 \pm 0.09 \pm 0.33$	$2.35 \pm 0.01 \pm 0.67$
16	$0.55 \pm 0.07 \pm 0.21$	$1.08 \pm 0.01 \pm 0.40$
17	$0.35 \pm 0.06 \pm 0.28$	$0.71 \pm 0.01 \pm 0.54$
18	$0.24 \pm 0.05 \pm 0.12$	$0.45 \pm 0.01 \pm 0.21$
19	$0.09 \pm 0.04 \pm 0.13$	$0.17 \pm 0.01 \pm 0.24$
20	$0.07 \pm 0.04 \pm 0.02$	$0.14 \pm 0.01 \pm 0.05$

Table 7 Charged particle multiplicity distribution in the pseudorapidity range $2.0 < \eta < 4.5$ for minimum bias events and for hard QCD events (see text). The first quoted uncertainty is statistical and the second is systematic

n_{ch}	Prob. in min. bias events $\times 10^3$	Prob. in hard QCD events $\times 10^3$
1	$51.23 \pm 0.16 \pm 2.05$	$5.38 \pm 0.09 \pm 0.45$
2	$56.09 \pm 0.18 \pm 2.35$	$10.02 \pm 0.14 \pm 1.10$
3	$60.21 \pm 0.20 \pm 2.38$	$14.69 \pm 0.17 \pm 2.04$
4	$63.32 \pm 0.21 \pm 2.81$	$21.62 \pm 0.23 \pm 2.16$
5	$63.18 \pm 0.23 \pm 1.82$	$26.22 \pm 0.26 \pm 1.88$
6	$61.39 \pm 0.24 \pm 1.14$	$31.38 \pm 0.31 \pm 1.94$
7	$58.08 \pm 0.25 \pm 0.57$	$35.13 \pm 0.35 \pm 1.87$
8	$53.81 \pm 0.26 \pm 0.24$	$37.72 \pm 0.39 \pm 1.67$
9	$49.25 \pm 0.27 \pm 0.32$	$39.37 \pm 0.43 \pm 2.27$
10	$45.18 \pm 0.28 \pm 0.26$	$42.69 \pm 0.49 \pm 2.31$
11	$41.36 \pm 0.29 \pm 0.28$	$43.07 \pm 0.53 \pm 1.37$
12	$37.94 \pm 0.31 \pm 0.35$	$43.97 \pm 0.58 \pm 1.39$
13	$35.09 \pm 0.32 \pm 0.30$	$43.52 \pm 0.63 \pm 1.71$
14	$32.55 \pm 0.34 \pm 0.33$	$45.25 \pm 0.70 \pm 2.01$
15	$30.48 \pm 0.36 \pm 0.43$	$43.98 \pm 0.75 \pm 0.86$
16	$28.20 \pm 0.38 \pm 0.48$	$43.48 \pm 0.81 \pm 0.90$
17	$26.55 \pm 0.40 \pm 0.40$	$43.85 \pm 0.89 \pm 0.74$
18	$24.83 \pm 0.43 \pm 0.39$	$42.96 \pm 0.96 \pm 0.34$
19	$23.26 \pm 0.45 \pm 0.39$	$41.47 \pm 1.02 \pm 0.24$
20	$21.64 \pm 0.48 \pm 0.59$	$40.21 \pm 1.09 \pm 0.29$
21	$19.87 \pm 0.19 \pm 0.46$	$37.97 \pm 0.43 \pm 0.51$
23	$17.44 \pm 0.20 \pm 0.52$	$35.08 \pm 0.46 \pm 0.67$
25	$15.49 \pm 0.21 \pm 0.76$	$32.39 \pm 0.51 \pm 0.87$
27	$13.24 \pm 0.22 \pm 0.68$	$30.02 \pm 0.56 \pm 1.42$
29	$11.63 \pm 0.23 \pm 0.60$	$26.14 \pm 0.57 \pm 1.54$
31	$10.05 \pm 0.24 \pm 0.62$	$23.18 \pm 0.60 \pm 1.38$
33	$8.66 \pm 0.25 \pm 0.62$	$20.40 \pm 0.63 \pm 1.45$
35	$7.43 \pm 0.26 \pm 0.60$	$17.59 \pm 0.63 \pm 1.52$
37	$6.19 \pm 0.26 \pm 0.72$	$15.85 \pm 0.66 \pm 1.88$
39	$5.56 \pm 0.26 \pm 0.71$	$13.11 \pm 0.64 \pm 1.45$
41	$4.40 \pm 0.25 \pm 0.62$	$11.22 \pm 0.64 \pm 1.32$
43	$3.71 \pm 0.25 \pm 0.56$	$9.55 \pm 0.63 \pm 1.24$
45	$3.14 \pm 0.24 \pm 0.44$	$7.74 \pm 0.59 \pm 1.27$
47	$2.68 \pm 0.23 \pm 0.46$	$6.21 \pm 0.58 \pm 1.40$
49	$2.00 \pm 0.22 \pm 0.49$	$5.38 \pm 0.54 \pm 1.09$
51	$1.70 \pm 0.12 \pm 0.32$	$4.18 \pm 0.30 \pm 1.09$
54	$1.22 \pm 0.11 \pm 0.24$	$3.04 \pm 0.27 \pm 0.69$
57	$0.88 \pm 0.09 \pm 0.20$	$2.26 \pm 0.24 \pm 0.49$
60	$0.63 \pm 0.08 \pm 0.15$	$1.58 \pm 0.21 \pm 0.45$

References

1. K. Aamodt et al., Eur. Phys. J. C **68**, 345 (2010). doi:10.1140/epjc/s10052-010-1350-2
2. G. Aad et al., New J. Phys. **13**, 053033 (2011). doi:10.1088/1367-2630/13/5/053033
3. V. Khachatryan et al., J. High Energy Phys. **01**, 079 (2011). doi:10.1007/JHEP01(2011)079
4. R. Corke, T. Sjöstrand, J. High Energy Phys. **01**, 035 (2010). doi:10.1007/JHEP01(2010)035
5. A.A. Alves Jr. et al., J. Instrum. **3**, S08005 (2008). doi:10.1088/1748-0221/3/08/S08005
6. S. Agostinelli et al., Nucl. Instrum. Methods Phys. Res., Sect. A, Accel. Spectrom. Detect. Assoc. Equip. **506**, 250 (2003). doi:10.1016/S0168-9002(03)01368-8
7. T. Sjöstrand, S. Mrenna, P. Skands, J. High Energy Phys. **05**, 026 (2006). doi:10.1088/1126-6708/2006/05/026
8. J. Pumplin et al., J. High Energy Phys. **07**, 012 (2002)
9. I. Belyaev, T. Brambach, N.H. Brook, N. Gauvin, G. Corti, K. Harrison, P.F. Harrison, J. He, P.H. Hilten, C.R. Jones, M. Lieng, G. Manca, S. Miglioranzi, P. Robbe, V. Vagnoni, M. Whitehead, J. Wishahi, O. Steinkamp, F. Archilli, B. Sciascia, in *IEEE Nucl. Sci. Symp. Conf. Rec.* (2010), p. 1155
10. D.J. Lange, Nucl. Instrum. Methods Phys. Res., Sect. A, Accel. Spectrom. Detect. Assoc. Equip. **462**, 152 (2001). doi:10.1016/S0168-9002(01)00089-4
11. P. Golonka, Z. Wąs, Eur. Phys. J. C **45**, 97 (2006). doi:10.1140/epjc/s2005-02396-4
12. R. Aaij et al., Phys. Lett. B **693**, 69 (2010). doi:10.1016/j.physletb.2010.08.055
13. R. Aaij et al., J. High Energy Phys. **08**, 034 (2011). doi:10.1007/JHEP08(2011)034
14. A. Jaeger, P. Seyfert, M. De Cian, J. Tilburg, S. Hansmann-Menzemer, Tracking performance of the LHCb spectrometer (2011). http://cdsweb.cern.ch/record/1389493. LHCb-PROC-2011-057
15. P. Skands, Phys. Rev. D **82**, 074018 (2010). doi:10.1103/PhysRevD.82.074018
16. T. Sjöstrand, S. Mrenna, P. Skands, Comput. Phys. Commun. **178**, 852 (2008). doi:10.1016/j.cpc.2008.01.036
17. R. Engel, Z. Phys. C **66**, 203 (1995). doi:10.1007/BF01496594
18. Z. Koba, H.B. Nielsen, P. Olesen, Nucl. Phys. B **40**, 317 (1972). doi:10.1016/0550-3213(72)90551-2

The LHCb Collaboration

R. Aaij[23], C. Abellan Beteta[35,n], B. Adeva[36], M. Adinolfi[42], C. Adrover[6], A. Affolder[48], Z. Ajaltouni[5], J. Albrecht[37], F. Alessio[37], M. Alexander[47], G. Alkhazov[29], P. Alvarez Cartelle[36], A.A. Alves Jr[22], S. Amato[2], Y. Amhis[38], J. Anderson[39], R.B. Appleby[50], O. Aquines Gutierrez[10], F. Archilli[18,37], L. Arrabito[53,p], A. Artamonov[34], M. Artuso[52,37], E. Aslanides[6], G. Auriemma[22,m], S. Bachmann[11], J.J. Back[44], D.S. Bailey[50], V. Balagura[30,37], W. Baldini[16], R.J. Barlow[50], C. Barschel[37], S. Barsuk[7], W. Barter[43], A. Bates[47], C. Bauer[10], Th. Bauer[23], A. Bay[38], I. Bediaga[1], S. Belogurov[30], K. Belous[34], I. Belyaev[30,37], E. Ben-Haim[8], M. Benayoun[8], G. Bencivenni[18], S. Benson[46], J. Benton[42], R. Bernet[39], M.-O. Bettler[17], M. van Beuzekom[23], A. Bien[11], S. Bifani[12], T. Bird[50], A. Bizzeti[17,h], P.M. Bjørnstad[50], T. Blake[37], F. Blanc[38], C. Blanks[49], J. Blouw[11], S. Blusk[52], A. Bobrov[33], V. Bocci[22], A. Bondar[33], N. Bondar[29], W. Bonivento[15], S. Borghi[47,50], A. Borgia[52], T.J.V. Bowcock[48], C. Bozzi[16], T. Brambach[9], J. van den Brand[24], J. Bressieux[38], D. Brett[50], M. Britsch[10], T. Britton[52], N.H. Brook[42], H. Brown[48], A. Büchler-Germann[39], I. Burducea[28], A. Bursche[39], J. Buytaert[37], S. Cadeddu[15], O. Callot[7], M. Calvi[20,j], M. Calvo Gomez[35,n], A. Camboni[35], P. Campana[18,37], A. Carbone[14], G. Carboni[21,k], R. Cardinale[19,37,i], A. Cardini[15], L. Carson[49], K. Carvalho Akiba[2], G. Casse[48], M. Cattaneo[37], Ch. Cauet[9], M. Charles[51], Ph. Charpentier[37], N. Chiapolini[39], K. Ciba[37], X. Cid Vidal[36], G. Ciezarek[49], P.E.L. Clarke[46,37], M. Clemencic[37], H.V. Cliff[43], J. Closier[37], C. Coca[28], V. Coco[23], J. Cogan[6], P. Collins[37], A. Comerma-Montells[35], F. Constantin[28], G. Conti[38], A. Contu[51], A. Cook[42], M. Coombes[42], G. Corti[37], G.A. Cowan[38], R. Currie[46], B. D'Almagne[7], C. D'Ambrosio[37], P. David[8], P.N.Y. David[23], I. De Bonis[4], S. De Capua[21,k], M. De Cian[39], F. De Lorenzi[12], J.M. De Miranda[1], L. De Paula[2], P. De Simone[18], D. Decamp[4], M. Deckenhoff[9], H. Degaudenzi[38,37], M. Deissenroth[11], L. Del Buono[8], C. Deplano[15], D. Derkach[14,37], O. Deschamps[5], F. Dettori[24], J. Dickens[43], H. Dijkstra[37], P. Diniz Batista[1], F. Domingo Bonal[35,n], S. Donleavy[48], F. Dordei[11], A. Dosil Suárez[36], D. Dossett[44], A. Dovbnya[40], F. Dupertuis[38], R. Dzhelyadin[34], A. Dziurda[25], S. Easo[45], U. Egede[49], V. Egorychev[30], S. Eidelman[33], D. van Eijk[23], F. Eisele[11], S. Eisenhardt[46], R. Ekelhof[9], L. Eklund[47], Ch. Elsasser[39], D. Elsby[55], D. Esperante Pereira[36], L. Estève[43], A. Falabella[16,14,e], E. Fanchini[20,j], C. Färber[11], G. Fardell[46], C. Farinelli[23], S. Farry[12], V. Fave[38], V. Fernandez Albor[36], M. Ferro-Luzzi[37], S. Filippov[32], C. Fitzpatrick[46], M. Fontana[10], F. Fontanelli[19,i], R. Forty[37], M. Frank[37], C. Frei[37], M. Frosini[17,37,f], S. Furcas[20], A. Gallas Torreira[36], D. Galli[14,c], M. Gandelman[2], P. Gandini[51], Y. Gao[3], J-C. Garnier[37], J. Garofoli[52], J. Garra Tico[43], L. Garrido[35], D. Gascon[35], C. Gaspar[37], N. Gauvin[38], M. Gersabeck[37], T. Gershon[44,37], Ph. Ghez[4], V. Gibson[43], V.V. Gligorov[37], C. Göbel[54,q], D. Golubkov[30], A. Golutvin[49,30,37], A. Gomes[2], H. Gordon[51], M. Grabalosa Gándara[35], R. Graciani Diaz[35], L.A. Granado Cardoso[37], E. Graugés[35], G. Graziani[17], A. Grecu[28], E. Greening[51], S. Gregson[43], B. Gui[52], E. Gushchin[32], Yu. Guz[34], T. Gys[37],

G. Haefeli[38], C. Haen[37], S.C. Haines[43], T. Hampson[42], S. Hansmann-Menzemer[11], R. Harji[49], N. Harnew[51], J. Harrison[50], P.F. Harrison[44], J. He[7], V. Heijne[23], K. Hennessy[48], P. Henrard[5], J.A. Hernando Morata[36], E. van Herwijnen[37], E. Hicks[48], K. Holubyev[11], P. Hopchev[4], W. Hulsbergen[23], P. Hunt[51], T. Huse[48], R.S. Huston[12], D. Hutchcroft[48], D. Hynds[47], V. Iakovenko[41], P. Ilten[12], J. Imong[42], R. Jacobsson[37], A. Jaeger[11], M. Jahjah Hussein[5], E. Jans[23], F. Jansen[23], P. Jaton[38], B. Jean-Marie[7], F. Jing[3], M. John[51], D. Johnson[51], C.R. Jones[43], B. Jost[37], M. Kaballo[9], S. Kandybei[40], M. Karacson[37], T.M. Karbach[9], J. Keaveney[12], I.R. Kenyon[55], U. Kerzel[37], T. Ketel[24], A. Keune[38], B. Khanji[6], Y.M. Kim[46], M. Knecht[38], P. Koppenburg[23], A. Kozlinskiy[23], L. Kravchuk[32], K. Kreplin[11], M. Kreps[44], G. Krocker[11], P. Krokovny[11], F. Kruse[9], K. Kruzelecki[37], M. Kucharczyk[20,25,37,j], T. Kvaratskheliya[30,37], V.N. La Thi[38], D. Lacarrere[37], G. Lafferty[50], A. Lai[15], D. Lambert[46], R.W. Lambert[24], E. Lanciotti[37], G. Lanfranchi[18], C. Langenbruch[11], T. Latham[44], C. Lazzeroni[55], R. Le Gac[6], J. van Leerdam[23], J.-P. Lees[4], R. Lefèvre[5], A. Leflat[31,37], J. Lefrançois[7], O. Leroy[6], T. Lesiak[25], L. Li[3], L. Li Gioi[5], M. Lieng[9], M. Liles[48], R. Lindner[37], C. Linn[11], B. Liu[3], G. Liu[37], J.H. Lopes[2], E. Lopez Asamar[35], N. Lopez-March[38], H. Lu[38,3], J. Luisier[38], A. Mac Raighne[47], F. Machefert[7], I.V. Machikhiliyan[4,30], F. Maciuc[10], O. Maev[29,37], J. Magnin[1], S. Malde[51], R.M.D. Mamunur[37], G. Manca[15,d], G. Mancinelli[6], N. Mangiafave[43], U. Marconi[14], R. Märki[38], J. Marks[11], G. Martellotti[22], A. Martens[8], L. Martin[51], A. Martín Sánchez[7], D. Martinez Santos[37], A. Massafferri[1], Z. Mathe[12], C. Matteuzzi[20], M. Matveev[29], E. Maurice[6], B. Maynard[52], A. Mazurov[16,32,37], G. McGregor[50], R. McNulty[12], C. Mclean[14], M. Meissner[11], M. Merk[23], J. Merkel[9], R. Messi[21,k], S. Miglioranzi[37], D.A. Milanes[13,37], M.-N. Minard[4], J. Molina Rodriguez[54], S. Monteil[5], D. Moran[12], P. Morawski[25], R. Mountain[52], I. Mous[23], F. Muheim[46], K. Müller[39], R. Muresan[28,38], B. Muryn[26], B. Muster[38], M. Musy[35], J. Mylroie-Smith[48], P. Naik[42], T. Nakada[38], R. Nandakumar[45], I. Nasteva[1], M. Nedos[9], M. Needham[46], N. Neufeld[37], C. Nguyen-Mau[38,o], M. Nicol[7], V. Niess[5], N. Nikitin[31], A. Nomerotski[51], A. Novoselov[34], A. Oblakowska-Mucha[26], V. Obraztsov[34], S. Oggero[23], S. Ogilvy[47], O. Okhrimenko[41], R. Oldeman[15,d], M. Orlandea[28], J.M. Otalora Goicochea[2], P. Owen[49], K. Pal[52], J. Palacios[39], A. Palano[13,b], M. Palutan[18], J. Panman[37], A. Papanestis[45], M. Pappagallo[47], C. Parkes[47,37], C.J. Parkinson[49], G. Passaleva[17], G.D. Patel[48], M. Patel[49], S.K. Paterson[49], G.N. Patrick[45], C. Patrignani[19,i], C. Pavel-Nicorescu[28], A. Pazos Alvarez[36], A. Pellegrino[23], G. Penso[22,l], M. Pepe Altarelli[37], S. Perazzini[14,c], D.L. Perego[20,j], E. Perez Trigo[36], A. Pérez-Calero Yzquierdo[35], P. Perret[5], M. Perrin-Terrin[6], G. Pessina[20], A. Petrella[16,37], A. Petrolini[19,i], A. Phan[52], E. Picatoste Olloqui[35], B. Pie Valls[35], B. Pietrzyk[4], T. Pilař[44], D. Pinci[22], R. Plackett[47], S. Playfer[46], M. Plo Casasus[36], G. Polok[25], A. Poluektov[44,33], E. Polycarpo[2], D. Popov[10], B. Popovici[28], C. Potterat[35], A. Powell[51], T. du Pree[23], J. Prisciandaro[38], V. Pugatch[41], A. Puig Navarro[35], W. Qian[52], J.H. Rademacker[42], B. Rakotomiaramanana[38], M.S. Rangel[2], I. Raniuk[40], G. Raven[24], S. Redford[51], M.M. Reid[44], A.C. dos Reis[1], S. Ricciardi[45], K. Rinnert[48], D.A. Roa Romero[5], P. Robbe[7], E. Rodrigues[47,50], F. Rodrigues[2], P. Rodriguez Perez[36], G.J. Rogers[43], S. Roiser[37], V. Romanovsky[34], M. Rosello[35,n], J. Rouvinet[38], T. Ruf[37], H. Ruiz[35], G. Sabatino[21,k], J.J. Saborido Silva[36], N. Sagidova[29], P. Sail[47], B. Saitta[15,d], C. Salzmann[39], M. Sannino[19,i], R. Santacesaria[22], C. Santamarina Rios[36], R. Santinelli[37], E. Santovetti[21,k], M. Sapunov[6], A. Sarti[18,l], C. Satriano[22,m], A. Satta[21], M. Savrie[16,e], D. Savrina[30], P. Schaack[49], M. Schiller[24], S. Schleich[9], M. Schlupp[9], M. Schmelling[10], B. Schmidt[37], O. Schneider[38], A. Schopper[37], M.-H. Schune[7], R. Schwemmer[37], B. Sciascia[18], A. Sciubba[18,l], M. Seco[36], A. Semennikov[30], K. Senderowska[26], I. Sepp[49], N. Serra[39], J. Serrano[6], P. Seyfert[11], B. Shao[3], M. Shapkin[34], I. Shapoval[40,37], P. Shatalov[30], Y. Shcheglov[29], T. Shears[48], L. Shekhtman[33], O. Shevchenko[40], V. Shevchenko[30], A. Shires[49], R. Silva Coutinho[44], T. Skwarnicki[52], A.C. Smith[37], N.A. Smith[48], E. Smith[51,45], K. Sobczak[5], F.J.P. Soler[47], A. Solomin[42], F. Soomro[18], B. Souza De Paula[2], B. Spaan[9], A. Sparkes[46], P. Spradlin[47], F. Stagni[37], S. Stahl[11], O. Steinkamp[39], S. Stoica[28], S. Stone[52,37], B. Storaci[23], M. Straticiuc[28], U. Straumann[39], V.K. Subbiah[37], S. Swientek[9], M. Szczekowski[27], P. Szczypka[38], T. Szumlak[26], S. T'Jampens[4], E. Teodorescu[28], F. Teubert[37], C. Thomas[51], E. Thomas[37], J. van Tilburg[11], V. Tisserand[4], M. Tobin[39], S. Topp-Joergensen[51], N. Torr[51], E. Tournefier[4,49], M.T. Tran[38], A. Tsaregorodtsev[6], N. Tuning[23], M. Ubeda Garcia[37], A. Ukleja[27], P. Urquijo[52], U. Uwer[11], V. Vagnoni[14], G. Valenti[14], R. Vazquez Gomez[35], P. Vazquez Regueiro[36], S. Vecchi[16], J.J. Velthuis[42], M. Veltri[17,g], B. Viaud[7], I. Videau[7], X. Vilasis-Cardona[35,n], J. Visniakov[36], A. Vollhardt[39], D. Volyanskyy[10], D. Voong[42], A. Vorobyev[29], H. Voss[10], S. Wandernoth[11], J. Wang[52], D.R. Ward[43], N.K. Watson[55], A.D. Webber[50], D. Websdale[49], M. Whitehead[44], D. Wiedner[11], L. Wiggers[23], G. Wilkinson[51], M.P. Williams[44,45], M. Williams[49], F.F. Wilson[45], J. Wishahi[9], M. Witek[25], W. Witzeling[37], S.A. Wotton[43], K. Wyllie[37], Y. Xie[46], F. Xing[51], Z. Xing[52], Z. Yang[3], R. Young[46], O. Yushchenko[34], M. Zavertyaev[10,a], F. Zhang[3], L. Zhang[52], W.C. Zhang[12], Y. Zhang[3], A. Zhelezov[11], L. Zhong[3], E. Zverev[31], A. Zvyagin[37]

[1]Centro Brasileiro de Pesquisas Físicas (CBPF), Rio de Janeiro, Brazil

[2]Universidade Federal do Rio de Janeiro (UFRJ), Rio de Janeiro, Brazil

[3]Center for High Energy Physics, Tsinghua University, Beijing, China

[4]LAPP, Université de Savoie, CNRS/IN2P3, Annecy-Le-Vieux, France

[5]Clermont Université, Université Blaise Pascal, CNRS/IN2P3, LPC, Clermont-Ferrand, France

[6]CPPM, Aix-Marseille Université, CNRS/IN2P3, Marseille, France

[7]LAL, Université Paris-Sud, CNRS/IN2P3, Orsay, France

[8]LPNHE, Université Pierre et Marie Curie, Université Paris Diderot, CNRS/IN2P3, Paris, France

[9]Fakultät Physik, Technische Universität Dortmund, Dortmund, Germany

[10]Max-Planck-Institut für Kernphysik (MPIK), Heidelberg, Germany

[11]Physikalisches Institut, Ruprecht-Karls-Universität Heidelberg, Heidelberg, Germany

[12]School of Physics, University College Dublin, Dublin, Ireland

[13]Sezione INFN di Bari, Bari, Italy

[14]Sezione INFN di Bologna, Bologna, Italy

[15]Sezione INFN di Cagliari, Cagliari, Italy

[16]Sezione INFN di Ferrara, Ferrara, Italy

[17]Sezione INFN di Firenze, Firenze, Italy

[18]Laboratori Nazionali dell'INFN di Frascati, Frascati, Italy

[19]Sezione INFN di Genova, Genova, Italy

[20]Sezione INFN di Milano Bicocca, Milano, Italy

[21]Sezione INFN di Roma Tor Vergata, Roma, Italy

[22]Sezione INFN di Roma La Sapienza, Roma, Italy

[23]Nikhef National Institute for Subatomic Physics, Amsterdam, The Netherlands

[24]Nikhef National Institute for Subatomic Physics and Vrije Universiteit, Amsterdam, The Netherlands

[25]Henryk Niewodniczanski Institute of Nuclear Physics Polish Academy of Sciences, Kracòw, Poland

[26]AGH University of Science and Technology, Kracòw, Poland

[27]Soltan Institute for Nuclear Studies, Warsaw, Poland

[28]Horia Hulubei National Institute of Physics and Nuclear Engineering, Bucharest-Magurele, Romania

[29]Petersburg Nuclear Physics Institute (PNPI), Gatchina, Russia

[30]Institute of Theoretical and Experimental Physics (ITEP), Moscow, Russia

[31]Institute of Nuclear Physics, Moscow State University (SINP MSU), Moscow, Russia

[32]Institute for Nuclear Research of the Russian Academy of Sciences (INR RAN), Moscow, Russia

[33]Budker Institute of Nuclear Physics (SB RAS) and Novosibirsk State University, Novosibirsk, Russia

[34]Institute for High Energy Physics (IHEP), Protvino, Russia

[35]Universitat de Barcelona, Barcelona, Spain

[36]Universidad de Santiago de Compostela, Santiago de Compostela, Spain

[37]European Organization for Nuclear Research (CERN), Geneva, Switzerland

[38]Ecole Polytechnique Fédérale de Lausanne (EPFL), Lausanne, Switzerland

[39]Physik-Institut, Universität Zürich, Zürich, Switzerland

[40]NSC Kharkiv Institute of Physics and Technology (NSC KIPT), Kharkiv, Ukraine

[41]Institute for Nuclear Research of the National Academy of Sciences (KINR), Kyiv, Ukraine

[42]H.H. Wills Physics Laboratory, University of Bristol, Bristol, United Kingdom

[43]Cavendish Laboratory, University of Cambridge, Cambridge, United Kingdom

[44]Department of Physics, University of Warwick, Coventry, United Kingdom

[45]STFC Rutherford Appleton Laboratory, Didcot, United Kingdom

[46]School of Physics and Astronomy, University of Edinburgh, Edinburgh, United Kingdom

[47]School of Physics and Astronomy, University of Glasgow, Glasgow, United Kingdom

[48]Oliver Lodge Laboratory, University of Liverpool, Liverpool, United Kingdom

[49]Imperial College London, London, United Kingdom

[50]School of Physics and Astronomy, University of Manchester, Manchester, United Kingdom

[51]Department of Physics, University of Oxford, Oxford, United Kingdom

[52]Syracuse University, Syracuse, NY, United States

[53]CC-IN2P3, CNRS/IN2P3, Lyon-Villeurbanne, France

[54]Pontifícia Universidade Católica do Rio de Janeiro (PUC-Rio), Rio de Janeiro, Brazil

[55]University of Birmingham, Birmingham, United Kingdom

[a]P.N. Lebedev Physical Institute, Russian Academy of Science (LPI RAS), Moscow, Russia

[b]Università di Bari, Bari, Italy

[c]Università di Bologna, Bologna, Italy

[d]Università di Cagliari, Cagliari, Italy

[e]Università di Ferrara, Ferrara, Italy

[f]Università di Firenze, Firenze, Italy

[g]Università di Urbino, Urbino, Italy

[h]Università di Modena e Reggio Emilia, Modena, Italy

[i]Università di Genova, Genova, Italy

[j]Università di Milano Bicocca, Milano, Italy

[k]Università di Roma Tor Vergata, Roma, Italy

[l]Università di Roma La Sapienza, Roma, Italy

[m]Università della Basilicata, Potenza, Italy

[n]LIFAELS, La Salle, Universitat Ramon Llull, Barcelona, Spain

[o]Hanoi University of Science, Hanoi, Viet Nam

[p]Associated member

[q]Associated to Universidade Federal do Rio de Janeiro (UFRJ), Rio de Janeiro, Brazil